The EMBO Journal Vol. 21 No. 9 pp. 2149–2158, 2002

Toxoplasma gondii myosin A and its light chain: a fast, single-headed, plus-end-directed motor

Angelika Herm-Götz[1], Stefan Weiss[2], Rolf Stratmann[1,3], Setsuko Fujita-Becker[4], Christine Ruff[5,6], Edgar Meyhöfer[5,6], Thierry Soldati[3,7], Dietmar J.Manstein[4], Michael A.Geeves[2] and Dominique Soldati[1,3,8]

[1]Zentrum für Molekulare Biologie, Universität Heidelberg, Im Neuenheimer Feld 282, [4]Department of Biophysics and [7]Department of Molecular Cell Research, Max-Plank-Institute for Medical Research, Jahnstrasse 29, D-69120 Heidelberg, [5]Department of Molecular and Cellular Physiology, Medical School Hanover, Carl-Neuberg Strasse 1, D-30625 Hanover, Germany and [2]Department of Biosciences, University of Kent, Canterbury CT2 7NJ, UK

[3]Present address: Department of Biological Sciences, Imperial College of Science, Technology and Medicine, Sir Alexander Fleming Building, Imperial College Road, London SW7 2AZ, UK
[6]Present address: Department of Mechanical Engineering, University of Michigan, 3130 G.G.Brown Building, 2350 Hayward Street, Ann Arbor, MI 48109-2125, USA

[8]Corresponding author
e-mail: d.soldati@ic.ac.uk

Successful host cell invasion is a prerequisite for survival of the obligate intracellular apicomplexan parasites and establishment of infection. *Toxoplasma gondii* penetrates host cells by an active process involving its own actomyosin system and which is distinct from induced phagocytosis. *Toxoplasma gondii* myosin A (TgMyoA) is presumed to achieve power gliding motion and host cell penetration by the capping of apically released adhesins towards the rear of the parasite. We report here an extensive biochemical characterization of the functional TgMyoA motor complex. TgMyoA is anchored at the plasma membrane and binds a novel type of myosin light chain (TgMLC1). Despite some unusual features, the kinetic and mechanical properties of TgMyoA are unexpectedly similar to those of fast skeletal muscle myosins. Microneedle–laser trap and sliding velocity assays established that TgMyoA moves in unitary steps of 5.3 nm with a velocity of 5.2 μm/s towards the plus end of actin filaments. TgMyoA is the first fast, single-headed myosin and fulfils all the requirements for power parasite gliding.

Keywords: invasion/myosin/myosin light chain/*Toxoplasma gondii*/transient kinetics

Introduction

The phylum of Apicomplexa consists mainly of medically and economically important pathogens that infect humans and animals. These obligate intracellular parasites actively penetrate their host in a few seconds by squeezing at 1–10 μm/s through a moving junction formed between the host cell and the parasite plasma membrane. Parasite replication then occurs safely within a non-fusogenic parasitophorous vacuole. The actomyosin-dependent gliding motility of *Toxoplasma gondii* tachyzoites and *Plasmodium* species sporozoites is an essential component of the invasion process (Sultan *et al*., 1997; Sibley *et al*., 1998). This unusual form of motility is not generated by the action of cilia or flagella but is probably driven by the redistribution of surface adhesin complexes towards the posterior pole of the parasite. The adhesive components of these complexes are presumed to establish a tight interaction with host cell receptors or extracellular matrix, while the cytoplasmic tail of the transmembrane proteins are anticipated to establish a direct or indirect connection with the actomyosin system (Dobrowolski and Sibley, 1996; Kappe *et al*., 1999). Time-lapse video microscopy revealed that *T.gondii* tachyzoites glide at a speed of 1–3 μm/s, based on a combination of three major modes of locomotion involving one or more myosin motor(s) (Hakansson *et al*., 1999). Five class XIV myosins have been identified so far in *T.gondii* (TgMyoA–E) (Heintzelman and Schwartzman, 1997; Hettmann *et al*., 2000; F.Delbac and D.Soldati, unpublished). While TgMyoB and TgMyoE are not expressed in tachyzoites, TgMyoC appears to play a role in parasite division (Delbac *et al*., 2001). The unique localization of TgMyoA at the plasma membrane makes it a primary candidate to propel the parasite into its host (Hettmann *et al*., 2000). Close homologues of TgMyoA are present in the genomes of *Plasmodium* spp. (Heintzelman and Schwartzman, 1997; Pinder *et al*., 1998; Hettmann *et al*., 2000; Matuschewski *et al*., 2001), *Eimeria* and *Theileria*.

Our accumulated evidence indicated that *TgMyoA* is an essential gene and important for parasite gliding and host cell invasion. Indeed, among other approaches, a second copy of *TgMyoA* was introduced under the control of a tetracycline repressor system (Meißner *et al*., 2001) and the endogenous copy was deleted by double homologous recombination. Unfortunately, due to an uncharacterized reversion mechanism, all survivors had lost the capacity to repress the expression of the inducible copy of TgMyoA by removal of anhydrotetracycline (data not shown). More recently, we have established a tet-transactivator (tTA) system for *T.gondii* and were able to disrupt the endogenous copy of *TgMyoA* successfully in the presence of a second copy controlled by a tTA-responsive promoter. Addition of anhydrotetracycline turns off expression of TgMyoA and prevents parasite gliding, host cell invasion and cell-to-cell spreading (M.Meissner, D.Schlüter and D.Soldati, manuscript submitted).

In a complementary approach to link TgMyoA to invasion mechanisms, we undertook a comprehensive dissection of its biochemical and biophysical properties. The motor(s) powering gliding is expected to be of a fast

type; however, TgMyoA, like all other class XIV myosins described so far, exhibits unusual structural features that call into question its ability to fulfil such a function. This myosin does not follow the TEDS rule (Bement and Mooseker, 1995), and the generally conserved glycine residue at the pivot point (Kinose *et al*., 1996) is replaced by a serine. We report here that TgMyoA is present at the plasma membrane associated with a novel type of light chain and that this single-headed myosin exhibits the kinetic properties, step size velocity and polarity of a fast conventional myosin II.

Results

Purification of TgMyoA and identification of the myosin light chain associated with the motor complex

To determine the biochemical and biophysical properties of this motor, full-length TgMyoA and TgMyoAΔtail (a mutant lacking 53 C-terminal residues) were purified from recombinant parasites. The apparent molecular mass of the two proteins was determined by glycerol gradient centrifugation (Figure 1A). As expected, TgMyoAΔtail fractionated close to its molecular size of ~100 kDa. In contrast, TgMyoA had an apparent size of 160 kDa, clearly smaller than a dimer, but nevertheless bigger than was predicted by the 53 residues difference between the two proteins. Despite the lack of clearly identifiable binding site in the neck/tail of TgMyoA, we searched for the presence of a light chain. The neck domains of many unconventional myosins bind calmodulin, therefore we raised specific antibodies against *T.gondii* calmodulin (TgCaM; previously described by Seeber *et al*., 1999). Association of TgCaM with TgMyoA or TgMyoAΔtail could be ruled out as they did not co-purify (Figure 1C) and did not co-fractionate on glycerol gradients (data not shown). Beside calmodulin, a calmodulin-like protein is present in the *P.falciparum* genome database as well as in several expressed sequence tag (EST) databases of other apicomplexan parasites including *T.gondii*. We cloned and characterized the gene coding for this *T.gondii* calmodulin-like protein and raised polyclonal antibodies against the first 75 amino acid residues of the protein fused to GST and expressed in *Escherichia coli.* The antisera detected a 31 kDa protein that, in contrast to TgCaM, co-fractionated with TgMyoA on the glycerol gradient (Figure 1A).

We conclude that, as predicted from the absence of a coiled-coil domain in the tail region, these experiments indicate that native TgMyoA is single headed (Figure 1A).

Further analysis by western blotting revealed that the 31 kDa protein co-purified with TgMyoA heavy chain in several native preparations but was absent when TgMyoA was purified under denaturing conditions or when native TgMyoAΔtail was purified (Figure 1B). Based on the characteristics defined in this study, we named this protein *T.gondii* myosin light chain 1 (TgMLC1). Consistent with the results obtained above, we also showed that the last 53 amino acid residues in the tail of TgMyoA were necessary and sufficient to bind TgMLC1 (Figure 1D). A stretch of His_8 tag was introduced at the N-terminus of green fluorescent protein (GFP) in the pTGFP and pTGFPAtail constructs (Hettmann *et al*., 2000). HisGFP and HisGFPAtail proteins were expressed stably in *T.gondii*

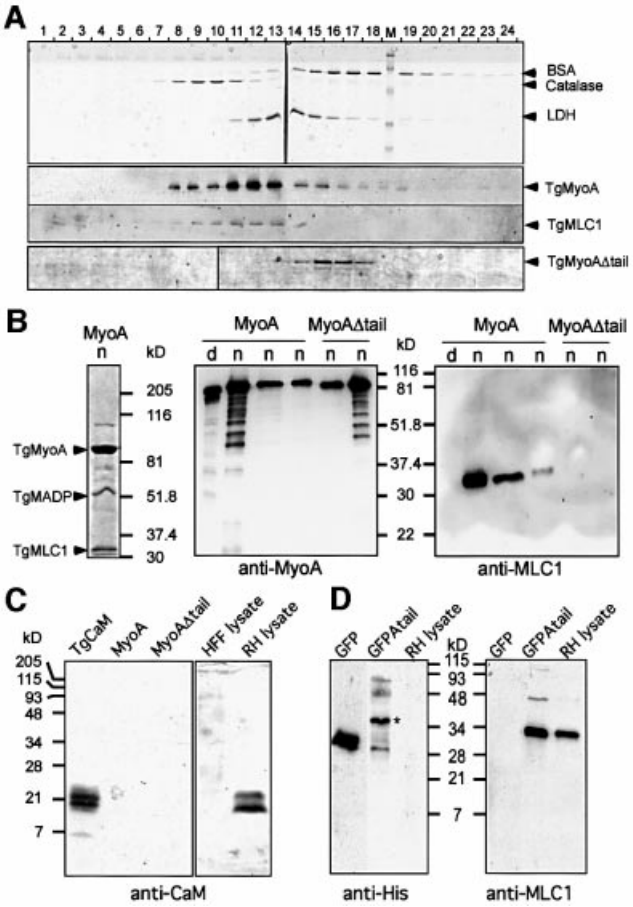

Fig. 1. Co-purification of TgMLC1 with TgMyoA as a 160 kDa complex. (**A**) Purified TgMyoA was fractionated through 10–30% glycerol gradients. Aliquots of each fraction were subjected to SDS–PAGE and immunoblotting using antibodies against TgMLC1 and TgMyoA. The two proteins co-fractionated and peaked at ~160 kDa (fractions 11–13). A control gradient with size makers was run in parallel and analysed by SDS–PAGE followed by Coomassie Blue staining. TgMyoAΔtail was analysed on an identical gradient and peaked at ~100 kDa (fractions 15–16). (**B**) Coomassie Blue-stained SDS–polyacrylamide gel of the purified TgMyoA under native conditions (left panel). Western blot analysis of several preparations of TgMyoA and TgMyoAΔtail purified on Ni-NTA columns under native (n) and denaturing (d) conditions using anti-MyoA (middle panel) and anti-MLC1 antibodies (right panel). TgMLC1 co-purified only with intact TgMyoA under native conditions. (**C**) Western blot analysis of purified native preparations of TgMyoA and TgMyoAΔtail using anti-TgCaM antibodies. TgCaM corresponds to bacterially expressed recombinant protein. The specificity of the anti-TgCaM antibodies was controlled on the left panel by analysing total lysates prepared from host cells (HFF, human foreskin fibroblast) and wild-type parasites (RH). (**D**) Western blot analysis of total RH lysates and purified fraction of HisGFP and HisGFPAtail (indicated by an asterisk on the gel) after elution from Ni-NTA resin. TgMLC1 is present in parasites' total lysate and co-purified with GFPAtail but not with GFP alone.

and purified from parasite lysates on Ni-NTA resin. TgMLC1 co-purified specifically with HisGFPAtail but not with HisGFP as detected by western blotting of the material eluted from the batch purification. Finally, additional data from another group allowed us to establish that the TgMyoA complex is at least heterotrimeric. It is composed of one TgMyoA heavy chain (93 kDa), one light chain (TgMLC1; 31 kDa) and a recently identified, 50 kDa myristoylated protein (TgMADP) which anchors TgMyoA at the plasma membrane (C.Beckers, International

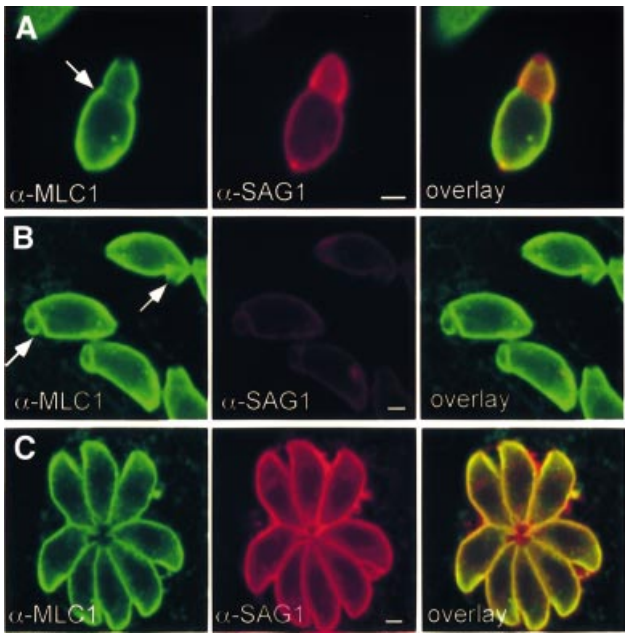

Fig. 2. Subcellular distribution of TgMLC1 during parasite penetration of host cells. Double indirect immunofluorescence using differential permeabilization was analysed by confocal microscopy. The major surface antigen (SAG1) is detected prior to permeabilization to label the extracellular portion of the penetrating parasites preferentially, while TgMLC1 was visualized after permeabilization (Triton X-100, 0.2%). (**A**) Partial penetration of parasites attached to the host surface. The arrow indicates the site of the moving junction. (**B**) Less than 10 min after invasion, intracellular parasites are not stainable with anti-SAG1 without permeabilization. The arrows point to the posterior end of the parasites. (**C**) At 24 h post-invasion, a double immunofluorescence with anti-MLC1 and anti-SAG1 under permeabilized conditions showed co-localization of both proteins. Scale bar: 1 μm.

Meeting on Toxoplasmosis, Freising, 2001). Using anti-TgMADP antibodies, we observed that the docking protein co-purified with TgMyoA under exactly the same conditions as TgMLC1 (data not shown).

TgMLC1 co-localized with TgMyoA at the parasite plasma membrane

As anticipated for a TgMyoA-associated protein, TgMLC1 localized at the parasite plasma membrane under static conditions (intracellular parasites) (Figure 2C). In addition, during host cell penetration, TgMLC1 was slightly concentrated at the moving junction and in the part of the parasite penetrating the host cell (Figure 2A). Less than 10 min later, TgMLC1 was still distributed at the parasite periphery but also revealed a circle at the posterior end, delineating an open 'appendage' at the parasite posterior extremity (Figure 2B). This structure, visible only shortly after invasion, is likely to correspond to the transient posterior invagination where multi-lamellar vesicles are released to form the intravacuolar network (Sibley et al 1995).

TgMyoA binds a novel type of light chain and both proteins are restrictively conserved throughout the Apicomplexa

TgMLC1 comprises 213 amino acids and appears to be composed of four degenerate EF hand domains (Figure 3A). Structural homology searches indicated that only the third one (residues 149–179) fits the consensus sequence well; the first one is relatively conserved but the other two carry multiple deletions. Very closely related proteins of similar sizes are present in the genome of several Apicomplexa and most probably correspond to the light chain of MyoA homologues. The N-terminal 60 residues are unique, not present in calmodulin or other myosin light chains and highly conserved in the Apicomplexa. TgMyoAΔtail was shown to be cytosolic, and the determinant of plasma membrane localization of TgMyoA mapped within its last 22 residues and was strictly dependent on an RR motif (Hettmann *et al*., 2000) (see Figure 3B, bar and double arrowhead). Interestingly, deletion of the tail prevents co-purification of TgMLC1 and TgMADP. Close examination of the last 22 residues reveals the presence of a very degenerate IQ motif (QXXXR, Figure 3B). The precise topology of the TgMyoA–TgMLC1–TgMADP complex remains to be determined.

Transient kinetics of TgMyoA ATPase

The heterotrimeric TgMyoA complex could only be purified in very small amounts, which were insufficient for kinetic analysis using stopped-flow methods but were ample for use in the flash photolysis system developed for limited quantities of myosins (Weiss *et al*., 2000). In contrast, transient kinetic data for monomeric TgMyoAΔtail were acquired by both stopped-flow and flash photolysis methods. The maximum velocity at which myosins move over actin is normally limited by the net rate of cross-bridge detachment at the end of the power stroke (Siemankowski and White, 1984; Weiss *et al*., 2001). This detachment rate can be limited by the rates of both ADP release and ATP binding, measurements of which can therefore be diagnostic of maximum gliding velocity. The rate constant of the ATP-induced dissociation of both full-length TgMyoA and TgMyoAΔtail from actin was determined by the flash photolysis method as shown in Figure 4A. A known concentration of ATP was released from 0.5 mM caged ATP in a sample 0.5 μM actin and 1 μM TgMyoA and the dissociation of the complex monitored by the decrease of the light scattering signal. A single exponential fit to the light scattering trace gave the k_{obs} of the reaction (Figure 4A). The experiment was repeated at various ATP concentrations and a plot of k_{obs} versus [ATP] was linear over the range of concentrations used. The slope of the linear regression defines the apparent second-order rate constant K_1k_{+2} = 0.28 and 0.46/μM/s for full-length TgMyoA and TgMyoAΔtail, respectively (Figure 4B).

The affinity of ADP for acto·TgMyoA was measured from the ADP inhibition of the ATP dissociation experiment. A constant 50 μM ATP was photoreleased in the presence of increasing amounts of ADP (0 μM–2 mM). The value of k_{obs} decreased as the ADP concentration increased, and the resulting data were described by a hyperbola (Scheme I, see Table I footnotes), suggesting that ADP binding and dissociation is in rapid equilibrium with acto·TgMyoA preceding ATP-induced dissociation of the complex (Scheme II). The analysis defined the ADP affinity, K_{AD}, as 840 and 720 μM for TgMyoA and TgMyoAΔtail, respectively (Figure 4C). The flash photo-

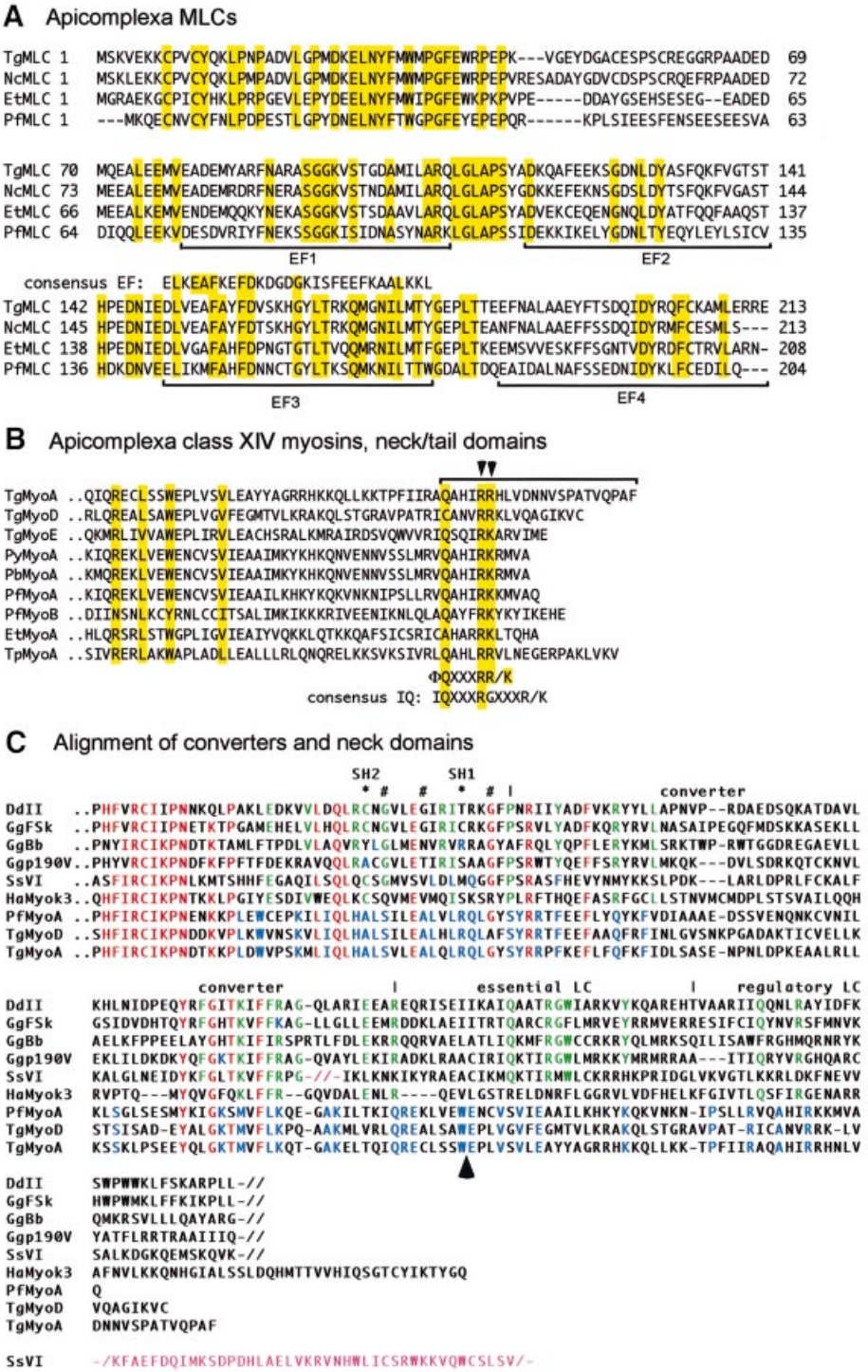

Fig. 3. Sequence alignments of apicomplexan myosin light and heavy chains. (**A**) Myosin light chains from *P.falciparum*, *Eimeria tenella*, *Neospora caninum* and *T.gondii*. TgMLC1 accession No. AY048862. The position of the four proposed degenerate EF hand domains is indicated by a bar. (**B**) Alignment of the C-terminus of class XIV myosin heavy chains from *T.gondii*, *Plasmodium* spp., *E.tenella* and *Theileira parva*. (**C**) Alignment of myosin sequences around the converter domain and the lever arm helix of selected myosins of different classes that have been characterized biochemically, except PfMyoA. Myosin VI is the only minus-end-directed myosin characterized so far. The alignment starts at position 650 of *D.discoideum* myosin II and ends at residue 821. The arrowhead indicates where the TgMyoAΔtail was truncated. The structural domains are indicated at the top of the alignment, as described by Geeves and Holmes (1999). The asterisk indicates two cysteines (SH1, SH2) conserved in class II myosins; the hash sign indicates three glycines conserved among most myosin classes. The first glycine is the proposed 'pivot point' corresponding to Gly699 of GgFSk (Kinose *et al*., 1996), and is absolutely conserved except in a plant myosin (HaMyok3) and a *Caenorhabditis elegans* class XII myosin. Conservation between class XIV myosins and others is highest upstream of and including the actin-binding domain. Residues conserved in at least six of eight sequences are in red; residues conserved in at least four of the five non-class XIV myosins are in green; and the C-terminus highly conserved among class XIV myosins is in blue. The myosin VI-specific insertion at the end of the converter domain is cut out of the alignment and presented below in pink. *Dictyostelium discoideum* myosin II (DdII, accession No. P08799); *Gallus gallus* (chicken) fast skeletal myosin II (GgFsk, P13538); *G.gallus* brush border myosin I (GgBb, U04049); *G.gallus* p190 myosin V (Ggp190V, Z11718); *Sus scrofa domestica* myosin VI (SsVI, A54818); *P.falciparum* myosin A (PfMyoA, AAD21242); *T.gondii* myosin D (TgMyoD, AF105118); *T.gondii* myosin A (TgMyoA, AAC47724).

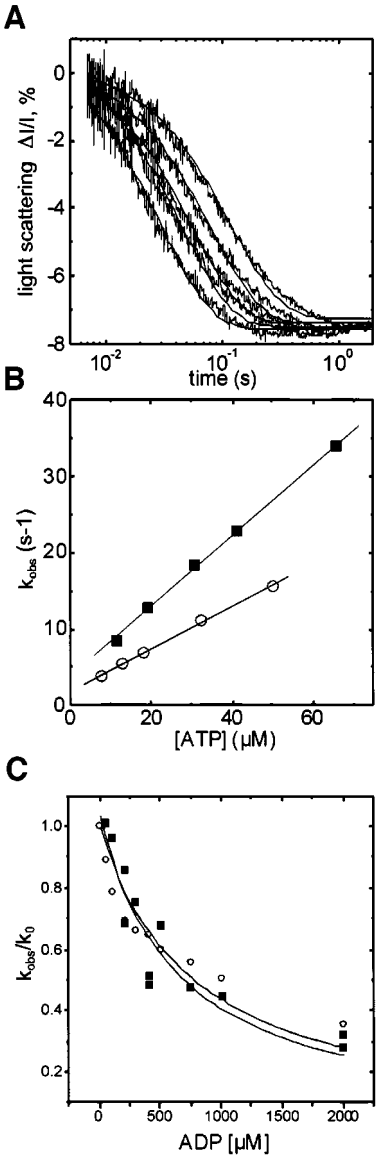

Fig. 4. Transient kinetics of TgMyoA ATPase. ATP induced dissociation of actin from TgMyoAΔtail and full-length TgMyoA in flash photolysis. (**A**) Light scattering signals from a 20 μl sample containing 0.5 μM actin, 1 μM TgMyoAΔtail, 0.5 mM ATP and apyrase in a multiple flash experiment. The best fit to a single exponential decay of the light scattering decrease is shown superimposed. (**B**) The observed rate constants of ATP-induced dissociation, k_{obs}, of TgMyoAΔtail (filled squares) and full-length TgMyoA (open circles) are plotted versus the concentration of ATP released. The slope of a linear fit to each set of data from one isoform gives a second-order rate constant (K_1k_{+2}) of 0.46 ± 0.01/μM/s with an intercept of 3.8 ± 0.4/s for TgMyoAΔtail. For full-length TgMyoA, the linear fit gives a second-order rate constant (K_1k_{+2}) of 0.28 ± 0.005/μM/s with an intercept of 0.17 ± 0.2/s. Other conditions: experimental buffer containing 130 mM KCl, 20 mM MOPS, 5 mM $MgCl_2$ and 10 mM fresh DTT at pH 7.0 and 22°C. (**C**) ADP affinity for acto·TgMyoAΔtail and full-length acto·TgMyoA. The inhibition of the k_{obs} for ATP-induced dissociation of actomyosin is plotted versus the concentration of ADP for TgMyoAΔtail (filled squares) and full-length TgMyoA (open circles). For easier comparison between the two data sets, all k_{obs} values were divided by k_0, the value of k_{obs} at 0 μM [ADP]. For each series of measurements, a fit to Equation 1 is superimposed, giving K_{AD} values of 840 ± 60 μM for TgMyoAΔtail and 720 ± 90 μM for full-length TgMyoA.

lysis experiments showed that the values of both K_1k_{+2} and K_{AD} were similar for TgMyoA and TgMyoAΔtail and demonstrate that the truncation of the tail by 53 residues does not alter the kinetic properties of the motor domain of TgMyoA.

A more complete kinetic characterization by stopped flow was then undertaken with the more readily available TgMyoAΔtail. The ATP-induced dissociation and the ADP inhibition of the dissociation were measured using 400 nM acto·TgMyoA complex. Unlike any other myosin so far examined, TgMyoA (and TgMyoAΔtail) did not quench the fluorescence of a pyrene label covalently attached to actin. Therefore, dissociation of the complex was measured by light scattering. The results are given in Table I and although the stopped-flow measurements resulted in a higher value of K_1k_{+2} and a lower value of K_{AD} than flash photolysis, the values are of the same order for both methods. The data confirm that TgMyoA is dissociated quickly from actin by ATP and that the TgMyoA·actin complex has a low affinity for ADP, properties that TgMyoA shares with fast muscle myosins.

The rate of ATP binding to TgMyoAΔtail was determined by measuring the intrinsic tryptophan fluorescence change which occurs on ATP binding. A 3% decrease in fluorescence was observed compared with the usual fluorescence increase obtained for other myosins, probably due to the absence of the tryptophan normally thought to be responsible (Batra and Manstein, 1999). The slope of the linear fit to a plot of k_{obs} versus [ATP] gives K_1k_{+2} = 0.72/μM/s (Table I). The measurement was repeated using the fluorescent analogues mantATP and mantADP and gave similar second-order binding rate constants. For ADP, the dissociation rate constant was estimated by displacing bound mantADP with a large excess of ATP, resulting in a value of k_{+6} = 0.95/s. The affinity of TgMyoA for mantADP was estimated as 2 μM from the relationship $K_D = K_7k_{+6}/k_{-6}$. The affinity of actin for TgMyoA was measured in a competition experiment with rabbit myosin S1. Under the conditions used, TgMyoA had a 2- to 3-fold lower affinity for actin than S1. Under physiological conditions, the dissociation equilibrium constant (K_A) of S1 for actin is 30 nM, suggesting a value of 60–90 nM for TgMyoA·actin. To determine ATP turnover activity of TgMyoAΔtail, 50 nM TgMyoAΔtail with 50 or 200 μM ATP were quenched at various time points. The analysis of [ATP]/[ADP] ratios with an HPLC system gave an ATP turnover rate of 0.07/s in the absence and 1.5/s in the presence of 20 μM actin. A >20-fold activation in the presence of actin is typical of fast myosins.

Determination of TgMyoA velocity and step size

To complement this analysis, we directly determined some of the functional properties of this motor. The sliding velocity of actin filaments was measured in a standard *in vitro* motility assay (Kron and Spudich, 1986). We measured an average velocity of 5.2 μm/s for TgMyoA (Figure 5A). TgMyoAΔtail showed no motility under the same conditions, although the protein displayed ATP-dependent binding to actin. This lack of motility is probably due to a functional defect caused by deletion of the last 53 C-terminal residues, which hampers association with TgMLC1. The sequences of class XIV myosins diverge from that of other myosins, starting at a position corresponding to the SH1–SH2 region, just downstream of the 50k–20k domain junction (Figure 3C). Thus, TgMyoA

Table I. Transient kinetic analysis of nucleotide binding to TgMyoA and TgMyoAΔtail and actomyosin complexes

	Rate/equation constant	Units	TgMyoAΔtail	TgMyoA full	Dicty M76 1-2R	$Ch^{sm}S1$	$Rb^{st}S1$
Nucleotide binding	K_1k_{+2}	(/μM/s)	0.6		0.16	0.47	2.1
to acto·M	(FP) K_1k_{+2}	(/μM/s)	0.46	0.28			
	K_{AD}	(μM)	350		215	5	200
	(FP) K_{AD}	(μM)	720	840	–	–	–
mantADP	k_{-6}/K_7	(μM/s)	0.47		0.67	2	2.3
	k_{+6}	(/s)	0.95		2.6	0.13	0.23
	K_D	(μM)	2.0		3.9	0.075	0.1
ATP binding	K_1k_{+2}	(/μM/s)	1.1		1.1	2.1	2.3
mantATP	K_1k_{+2}	(/μM/s)	0.65		–	–	3.2
	K_{AD}/K_D		148		14.3	66	2000
Actin binding	K_A	(nM)	60–90		4.3	–	30

For comparison, parameters obtained for a genetically engineered *D.discoideum* myosin II catalytic fragment (Dicty M76 1-2R; Batra *et al*., 1999), chicken smooth muscle myosin II S1 ($Ch^{sm}S1$; Ritchie *et al*., 1993) and rabbit striated muscle myosin II S1 ($Rb^{st}S1$; Cremo and Geeves, 1998) are presented. The data marked (FP) were acquired by flash photolysis.

Scheme I

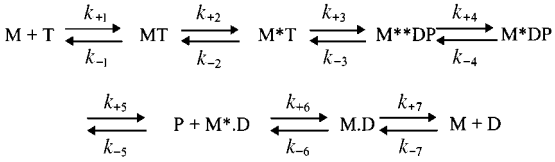

Scheme II

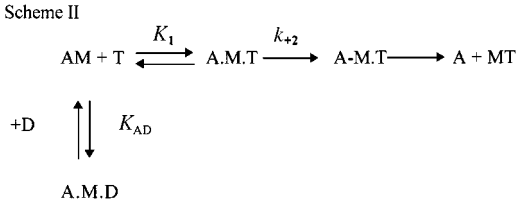

$$k_{obs} = \frac{k_{+2} \cdot K_1 \cdot [ATP]}{1 + [ADP]/K_{AD}} \qquad \text{Equation (1)}$$

displays little sequence similarity to other types of myosin in regions that normally form the converter and lever arm. The recent finding that myosin VI, exhibiting an unusual converter domain, is a minus-end-directed motor (Wells *et al*., 1999) prompted us to determine the directionality of TgMyoA. For this purpose, the *in vitro* motility assay was performed with actin filaments labelled with Oregon green at their plus (barbed) ends. To block actin polymerization at the plus end of the labelled tips, they were generated in the presence of gelsolin (Figure 5B). TgMyoA moved these polarity-marked filaments so that the labelled end was at the back of the moving filament, demonstrating that TgMyoA, like myosin II, moves towards the plus end of F-actin.

Furthermore, we employed a combined microneedle–laser trap transducer (Ruff *et al*., 2001) and directly measured the step displacements generated by single TgMyoA molecules. In agreement with our kinetic analysis, TgMyoA interacted transiently with actin filaments. A histogram analysis of 598 such interactions revealed an average step displacement of ~5.3 nm (Figure 6), comparable with the step size reported for myosin II (Veigel *et al*., 1999). In addition, these measurements confirm at the single molecule level that TgMyoA is a non-processive motor. Taken together, the sliding velocity and step size measurements of full-length TgMyoA are in perfect agreement with, and thus validate, the kinetic values.

Discussion

The catalytic domains and neck regions are remarkably conserved between myosin classes. Even in myosin VI, which displays motility towards the pointed end of actin filaments, there is clear structural conservation throughout most of the catalytic domain. TgMyoA shows some unusual features such as the lack of a glycine in the SH1 helix, a degenerate IQ motif and a low degree of sequence similarity with the converter region of conventional myosins. However, these differences are not sufficient to infer that TgMyoA lacks classical converter and light chain-binding domains that act as a conformational amplifier. Generally, the converter domains of myosins are not well conserved between classes outside a few critical residues. Functional conservation is suggested by the fact that most of the conserved hydrophobic residues in TgMyoA are found buried between the relay loop and the converter domain, where they play an essential role for the transmission of information between the nucleotide-binding site, the actin-binding site and the lever arm (Geeves and Holmes, 1999). This study established that TgMyoA, despite some unusual features, fulfils the

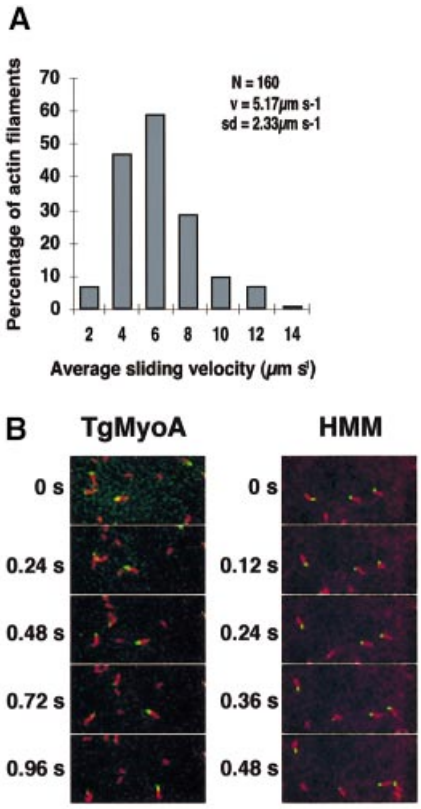

Fig. 5. Sliding velocity of actin filaments. (**A**) Histogram of the distribution of velocities of actin filaments sliding in the *in vitro* motility assay over TgMyoA. Only filaments with a minimal run length of 10 µm were scored. N, number of filaments; v, velocity; sd, standard deviation. (**B**) The directionality of TgMyoA movement was determined by the sliding of polarity-labelled actin filaments over a TgMyoA-decorated surface.

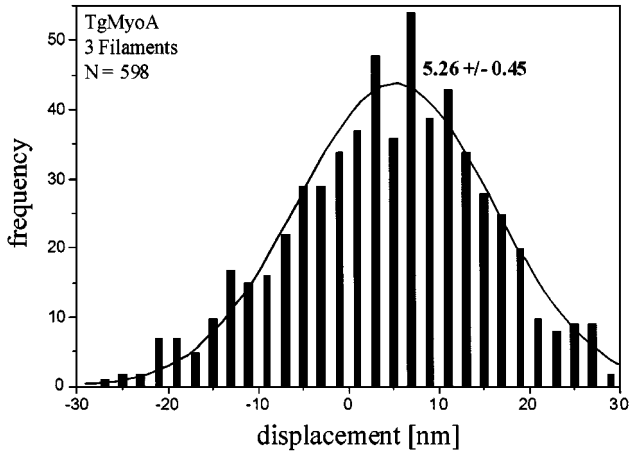

Fig. 6. Determination of the step size. The frequency distribution of displacements resulting from 598 interactions of single TgMyoA molecules with single actin filaments. To obtain a sufficiently large number, events were pooled from three independent recordings with single actin filaments that allowed unambiguous determination of the direction of the events. The shift in the fitted Gaussian distribution (solid line) was interpreted as the step size (Ruff *et al*., 2001). The estimated step size of TgMyoA was 5.26 ± 0.45 nm.

biochemical requirements for a fast motor involved in gliding (King, 1988; Hakansson *et al*., 1999). Like fast muscle myosins, TgMyoA has a short 'duty cycle', is thus non-processive and most probably operates in the context of large motor arrays. The fast release of ADP suggests that for this myosin, like other fast myosins, the rate-limiting step is either the phosphate release step or a preceding step such as the ATP cleavage. At an ATP concentration of 1 µM, we observed an average lifetime of the events of ~350 ms. This event duration is similar to the one we previously observed under identical conditions for skeletal muscle myosin (Ruff *et al*., 2001) and is also in good agreement with our kinetic analysis.

We provide here biochemical evidence that eliminates the possiblility that TgCaM serves as light chain for this myosin of the class XIV. Furthermore, both the solubility and localization of TgCaM in the parasites are not compatible with an association with TgMyoA (data not shown). Instead, we identified a novel type of light chain bound to the last 53 amino acids at the C-terminus of TgMyoA heavy chain. TgMyoA associated with TgMLC1 and TgMADP is distributed homogeneously beneath the parasite's plasma membrane (Hettmann *et al*., 2000), ready for a consolidated action. In accordance with the 'capping model' for invasion (Sibley *et al*., 1998), the directionality of TgMyoA implies that the actin filaments ought to be oriented with their plus ends toward the posterior pole. Surprisingly, both fluorescent phalloidin staining and sedimentation of crude cytoskeleton failed to detect actin filaments in parasites (Dobrowolski *et al*., 1997). This indicates that filaments might be very short and possibly undergo high turnover due to the abundant presence of actin-depolymerizing factors (Allen *et al*., 1997), and polymerize only in response to signalling generated by host cell contact at the time of invasion. Recently, treatment of parasites with the actin filament-stabilizing drug jasplakinolide was shown to induce an acrosomal process. Although actin filaments were clearly visible under these non-physiological conditions, their polarity could not be resolved (Shaw and Tilney, 1999)

The elaborate gliding motions of apicomplexan parasites accompanying host cell penetration allow entry significantly more quickly than by passive uptake via phagocytosis by host cells (Morisaki *et al*., 1995). This specific adaptation may serve as a selective escape mechanism, leading to the formation of a unique vacuole unable to fuse with endocytic compartments (Joiner *et al*., 1990). To accomplish such a fast process, one might speculate that the apicomplexans have learned to exploit the actin cytoskeleton fully, using a combination of myosin-powered motion together with the force generated directly by actin polymerization (reviewed in Theriot, 2000).

Materials and methods

Parasites strains, cell culture and reagents

Transgenic *T.gondii* parasites expressing the constructs pS·TgMyoA-tail and pS·TgMyoA were used as a source of recombinant proteins (Hettmann *et al*., 2000). *Toxoplasma gondii* tachyzoites were grown in Vero cells (African green monkey kidney cells) in tissue culture flasks, maintained in Dulbecco's modified Eagle's medium (DMEM) supplemented with 10% fetal calf serum (FCS), 2 mM glutamine and 25 µg/ml gentamicin. Rabbit polyclonal antibodies were raised against a bacterially

expressed GST fusion of 75 amino acids corresponding to the N-terminus of TgMLC1.

Protein purification

TgMyoAΔtail was purified as described previously (Hettmann *et al*., 2000). Full-length His-tagged TgMyoA was purified similarly with the following modifications. The parasite pellet (10^{10} parasites) was lysed by sonification in a buffer with detergent [2% Triton X-100, 4 mM ATP, 2 mM $MgCl_2$, 0.5 mM dithiothreitol (DTT), pH 7.6 and 1× Complete protease inhibitor cocktail (Roche)]. The suspension was clarified by ultracentrifugation at 65 000 r.p.m. and the supernatant was applied to an Ni-NTA resin column and eluted according to the manufacturer (The QIAexpressionist) (Janknecht *et al*., 1991). For the purification under denaturating conditions, the cells were lysed in the presence of 6 M guanidinium chloride and the clarified lysate was dialysed in the presence of 8 M urea before application on the column. Protein concentration was determined by a Bradford assay (Bio-Rad). SDS–PAGE was performed by standard methods. Average yields of 30 μg of TgMyoA and 250 μg of TgMyoAΔtail were obtained per gram of parasites. Active forms of TgMyoAΔtail and TgMyoA were purified further by co-precipitation with F-actin and release in the presence of ATP (Anson, 1992). Myosin subfragment 1 (S1) was prepared by chymotryptic digestion of rabbit myosin as described by Weeds and Taylor (1975). The molar concentration was determined from the extinction coefficient at 280 nm of $\varepsilon^{1\%} = 7.9$/cm and a molecular weight of 115 kDa. Rabbit skeletal actin was purified by the method of Spudich and Watt (1971). Its molar concentration was determined by absorbance at 280 nm ($\varepsilon^{1\%} = 1.104$/cm) and a molecular weight of 42 kDa (West *et al*., 1967). The preparation of pyrene-labelled actin was described previously (Criddle *et al*., 1985). To prepare phalloidin-stabilized F-actin (RhPh/actin), a stock solution of 10 μM F-actin and 10 μM phalloidin was incubated in experimental buffer overnight (Kurzawa and Geeves, 1996). Unless noted otherwise, all experiments with myosin S1 were performed in experimental buffer containing 100 mM KCl, 20 mM MOPS and 5 mM $MgCl_2$ at pH 7.0 and 20°C. In all flash photolysis experiments, fresh DTT was added to a concentration of 10 mM.

Glycerol gradient centrifugation

The centrifugation of 12 ml of glycerol density gradients was performed as described previously (Mitchell *et al*., 1997). The 10 and 30% glycerol solutions contained 50 mM NaH_2PO_4 and 300 mM NaCl pH 7.6. TgMyoA purified through the Ni-NTA column was loaded onto gradients after ultracentrifugation and overnight dialysis at 4°C against the 10% glycerol solution. A gradient was run in parallel with size standards: bovine serum albumin (BSA; 70 kDa), bovine catalase (240 kDa; Sigma) and beef heart lactate dehydrogenase (140 kDa; Roche). Fractions of 500 μl were collected and analysed by SDS–PAGE and western blot analysis.

Stopped-flow experiments

Stopped-flow experiments were performed with a Hi-Tech Scientific SF-61 DX2 stopped-flow spectrophotometer (Hi-Tech Scientific, Salisbury, UK) using procedures described previously (Ritchie *et al*., 1993; Cremo and Geeves, 1998; Furch *et al*., 1999). The affinity of TgMyoA for pyrene–actin was measured by competition with S1 (Coluccio and Geeves, 1999). The amplitude of the pyrene fluorescence change observed on dissociation of pyrA·S1 by addition of ATP gave a direct measure of the fraction of actin occupied by S1. Added TgMyoA competes with S1 for binding sites on actin, and analysis of the loss of amplitude defines the relative affinity of S1 and TgMyoA for actin.

Flash photolysis experiments

The optical bench for flash photolysis is designed for simultaneous time-resolved detection of transmission changes and either fluorescence or light scattering changes (Weiss *et al*., 2000). This system handles very small amounts of protein (<1 μg) in volumes of 10–20 μl, making experiments with the less efficiently purified TgMyoA possible.

HPLC-turnover experiments

The ATP turnover reaction for TgMyoA and acto·TgMyoA was measured by assaying the ATP/ADP ratio as a function of incubation time using HPLC analysis (Äkta Basic 10, Amersham Pharmacia Biotech with a 15 cm ODS-Hypersil column, run in 20 mM MOPS, 30 mM KCl and 5 mM $MgCl_2$ at pH 7.0). Samples in standard buffer (except 30 mM KCl) were quenched at various times by the addition of 2 μl of 6 M $HClO_4$ to 100 μl of sample and applied to the column after neutralization.

Determination of actin filament sliding velocity

Standard *in vitro* motility assays were performed as described previously (Furch *et al*., 1999). Assays were performed at 30°C in 25 mM imidazole·HCl pH 7.4, 25 mM KCl, 4 mM $MgCl_2$, 1 mM EGTA, 2 mM ATP and 10 mM DTT. All solutions were kept on ice prior to use and the microscope stage was stabilized at 30°C. A Zeiss Axiovert 135 inverted microscope with a 1.3 NA 40× oil immersion lens was used for epifluorescence with 540–550 nm excitation (100 W HBO) and 580 nm emission band-pass (Omega Optical filter set XF 37). Labelled actin filaments were imaged with a 1.3 NA 40× lens on an intensified video camera (Photonic Science Darkstar) and recorded, via an image processor (Hamamatsu Photonics, Argus 20) and time–date generator, by an S-VHS VCR (JVC BRS800-E). After focusing and observation of the actin filaments in rigor, motion was initiated by infusing 100 μl of buffer containing 2 mM ATP. For manual analyses, tapes were replayed from the VCR to the Argus 20 and individual filaments tracked frame-by-frame using a mouse. Velocity was calculated from the positional change and time code recorded on the tape. Experiments with TgMyoA and TgMyoAΔtail were performed with two freshly made protein preparations each. Chicken fast skeletal muscle HMM (8.5 ± 1.5 μm/s) and *Dictyostelium discoideum* myosin II (2.4 ± 0.3 μm/s) were used as positive controls and >100 filaments were analysed in each case. For protein preparation, see Ruppel *et al*. (1994) and Kron and Spudich (1986).

Preparation of polarity-labelled actin filament

Oregon green-labelled G-actin was mixed with gelsolin at a ratio of 33:1 and incubated on ice for 20 min. Adding 100 mM KCl at room temperature started actin polymerization. The resulting F-actin seeds were stabilized with phalloidin. Elongation of these seeds is restricted to the pointed end, because their barbed ends are blocked by gelsolin. For elongation, a 10-fold excess of unlabelled G-actin was added in Tris buffer containing 100 mM KCl, and the reaction was allowed to proceed for 15 min at room temperature. Finally, the polarity-labelled F-actin was diluted and the elongated part of the filaments was stabilized with rhodamine–phalloidin. An Olympus IX70 inverted microscope with a Zeiss 1.4 NA 100× oil immersion objective was used to image the filaments by epifluorescence. A Polychrom II monochromator (Till Photonics, Munich, Germany) in combination with a dual-band filter set (Chroma, Brattlesborough, USA) was used for excitation at 492 and 554 nm. Filaments were imaged using a Till Imago CCD camera, and TillVision was used for wavelength selection and image acquisition.

Step size measurements

Single actomyosin interactions were recorded with a combined microneedle–laser trap system as described previously (Ruff *et al*., 2001). This setup is similar to the double-laser trap system utilizing a three bead geometry (Finer *et al*., 1994), except that we replaced one of the trapped beads with a fine glass microneedle (stiffness 0.01–0.03 pN/nm, time constant ~1 ms). A magnified brightfield image of the needle projected onto a quadrant photo-diode (Hamamatsu, S1557) allows position detection with subnanometer resolution and a bandwidth of >8 kHz. Signals were low-pass filtered (1 kHz), sampled at 5 kHz with a microcomputer and stored on disk for off-line analysis. Single molecule *in vitro* assays were carried out in standard motility buffer (25 mM imidazole pH 7.4, 25 mM KCl, 1 mM EGTA, 4 mM $MgCl_2$, 1 μM ATP, 10 mM DTT, 100 μg/ml glucose oxidase, 18 μg/ml catalase and 3 mg/ml glucose). To record from a single TgMyoA motor, we constructed a recording chamber from two coverglasses that were separated by a 1 mm Teflon spacer. The lower coverglass was coated with a 0.1% nitrocellulose solution (Fullam Latham, NY) in amyl acetate containing 2.5 μm diameter silica beads (Bangs Laboratories, Fishers, IN) which served as pedestals. TgMgoA (1.5 μg/ml) was directly adsorbed onto nitrocellulose-coated surface by incubating for 15 min. We inserted a microneedle from the open side into the recording chamber and, using NEM-myosin as glue, attached a single actin filament at one end to the tip of the microneedle and at the other end to a 1 μm latex bead captured in the laser trap. The entire arrangement of microneedle, actin filament and latex bead was pulled taut, lowered carefully onto the myosin-coated bead and the ensuing actomyosin interactions were recorded. To determine the step size, we followed the strategy of Molloy *et al*. (1995). We identified single actomyosin interactions by a reduction of the thermal fluctuation of the microneedle sensor during binding to myosin. From the average position of a large number of such events, we calculated a histogram and determined the step size from the shift of the mean position of the distribution.

Acknowledgements

We would like to thank Dr T.Oda for gelsolin and helpful advice, Dr R.Goody for the supply of caged ATP and mant nucleotides, Dr Frank Seeber for providing us with *Tg gondii* calmodulin, Dr A.M.Estévez for technical assistance, and Dr Con Beckers for kindly providing anti-TgMADP antibodies and sharing information prior to publication. This work was funded mainly by grants from the Deutsche Forschungsgemeinschaft (D.S., T.S., E.M. and D.J.M.), The Volkswagen Stiftung (M.A.G. and D.J.M.) and the Wellcome Trust (M.A.G.).

References

Allen,M.L., Dobrowolski,J.M., Muller,H., Sibley,L.D. and Mansour,T.E. (1997) Cloning and characterization of actin depolymerizing factor from *Toxoplasma gondii*. *Mol. Biochem. Parasitol.*, **88**, 43–52.

Anson,M. (1992) Temperature dependence and Arrhenius activation energy of F-actin velocity generated *in vitro* by skeletal myosin. *J. Mol. Biol.*, **224**, 1029–1038.

Batra,R. and Manstein,D.J. (1999) Functional characterisation of *Dictyostelium* myosin II with conserved tryptophanyl residue 501 mutated to tyrosine. *Biol. Chem.*, **380**, 1017–1023.

Batra,R., Geeves,M.A. and Manstein,D.J. (1999) Kinetic analysis of *Dictyostelium discoideum* myosin motor domains with glycine-to-alanine mutations in the reactive thiol region. *Biochemistry*, **38**, 6126–6134.

Bement,W.M. and Mooseker,M.S. (1995) TEDS rule: a molecular rationale for differential regulation of myosins by phosphorylation of the heavy chain head. *Cell Motil. Cytoskeleton*, **31**, 87–92.

Coluccio,L.M. and Geeves,M.A. (1999) Transient kinetic analysis of the 130-kDa myosin I (*myr-1* gene product) from rat liver: a myosin designed for maintenance of tension? *J. Biol. Chem.*, **274**, 21575–21580.

Cremo,C.R. and Geeves,M.A. (1998) Interaction of actin and ADP with the head domain of smooth muscle myosin: implications for strain-dependent ADP release in smooth muscle. *Biochemistry*, **37**, 1969–1978.

Criddle,A.H., Geeves,M.A. and Jeffries,T. (1985) The use of actin labelled with *N*-(1-pyrenyl)iodoacetamide to study the interaction of actin with myosin subfragments and troponin/tropomyosin. *Biochem. J.*, **232**, 343–349.

Delbac,F. Sänger,A. Neuhaus,E., Ajioka,J. Toursel,C. Tomavo,S. Soldati,T. and Soldati,D. (2001) *Toxoplasma gondii* myosins B/C: one gene, two tails, two localizations and a role in parasite division. *J. Cell Biol.*, **155**, 613–623.

Dobrowolski,J.M. and Sibley,L.D. (1996) *Toxoplasma* invasion of mammalian cells is powered by the actin cytoskeleton of the parasite. *Cell*, **84**, 933–939.

Dobrowolski,J.M., Niesman,I.R. and Sibley,L.D. (1997) Actin in the parasite *Toxoplasma gondii* is encoded by a single copy gene, *ACT1* and exists primarily in a globular form. *Cell Motil. Cytoskeleton*, **37**, 253–262.

Finer,J.T., Simmons,R.M. and Spudich,J.A. (1994) Single myosin molecule mechanics: piconewton forces and nanometre steps. *Nature*, **368**, 113–119.

Furch,M., Fujita-Becker,S., Geeves,M.A., Holmes,K.C. and Manstein, D.J. (1999) Role of the salt-bridge between switch-1 and switch-2 of *Dictyostelium* myosin. *J. Mol. Biol.*, **290**, 797–809.

Geeves,M.A. and Holmes K.C. (1999) Structural mechanism of muscle contraction. *Annu. Rev. Biochem.*, **68**, 687–728.

Hakansson,S., Morisaki,H., Heuser,J. and Sibley,L.D. (1999) Time-lapse video microscopy of gliding motility in *Toxoplasma gondii* reveals a novel, biphasic mechanism of cell locomotion. *Mol. Biol. Cell*, **10**, 3539–3547.

Heintzelman,M.B. and Schwartzman,J.D. (1997) A novel class of unconventional myosins from *Toxoplasma gondii*. *J. Mol. Biol.*, **271**, 139–146.

Hettmann,C., Herm,A., Geiter,A., Frank,B., Schwarz,E., Soldati,T. and Soldati,D. (2000) A dibasic motif in the tail of a class XIV apicomplexan myosin is an essential determinant of plasma membrane localization. *Mol. Biol. Cell*, **11**, 1385–1400.

Janknecht,R., de Martynoff,G., Lou,J., Hipskind,R.A., Nordheim,A. and Stunnenberg,H.G. (1991) Rapid and efficient purification of native histidine-tagged protein expressed by recombinant vaccinia virus. *Proc. Natl Acad. Sci. USA*, **88**, 8972–8976.

Joiner,K.A., Fuhrman,S.A., Miettinen,H.M., Kasper,L.H. and Mellman,I. (1990) *Toxoplasma gondii*: fusion competence of parasitophorous vacuoles in Fc receptor-transfected fibroblasts. *Science*, **249**, 641–646.

Kappe,S., Bruderer,T., Gantt,S., Fujioka,H., Nussenzweig,V. and Menard,R. (1999) Conservation of a gliding motility and cell invasion machinery in apicomplexan parasites. *J. Cell Biol.*, **147**, 937–944.

King,C.A. (1988) Cell motility of sporozoan protozoa. *Parasitol. Today*, **11**, 315–318.

Kinose,F., Wang,S.X., Kidambi,U.S., Moncman,C.L. and Winkelmann, D.A. (1996) Glycine 699 is pivotal for the motor activity of skeletal muscle myosin. *J. Cell Biol.*, **134**, 895–909.

Kron,S.J. and Spudich,J.A. (1986) Fluorescent actin filaments move on myosin fixed to a glass surface. *Proc. Natl Acad. Sci. USA*, **83**, 6272–6276.

Kurzawa,S.E. and Geeves,M.A. (1996) A novel stopped-flow method for measuring the affinity of actin for myosin head fragments using microgram quantities of protein. *J. Muscle Res. Cell Motil.*, **17**, 669–676.

Matuschewski,K., Mota,M.M., Pinder,J.C., Nussenzweig,V. and Kappe, S.H. (2001) Identification of the class XIV myosins Pb-MyoA and Py-MyoA and expression in *Plasmodium*. *Mol. Biochem. Parasitol.*, **112**, 157–161.

Meißner,M., Brecht,S., Bujard,H. and Soldati,D. (2001) Modulation of myosin A expression by a newly established tetracycline repressor-based inducible system in *Toxoplasma gondii*. *Nucleic Acids Res.*, **29**, E115.

Mitchell,P., Petfalski,E., Shevchenko,A., Mann,M. and Tollervey,D. (1997) The exosome: a conserved eukaryotic RNA processing complex containing multiple 3′→5′ exoribonucleases. *Cell*, **91**, 457–466.

Molloy,J.E., Burns,J.E., Sparrow,J.C., Tregear,R.T., Kendrick-Jones,J. and White,D.C. (1995) Single-molecule mechanics of heavy meromyosin and S1 interacting with rabbit or *Drosophila* actins using optical tweezers. *Biophys. J.*, **68**, 298S–305S.

Morisaki,J.H., Heuser,J.E. and Sibley,L.D. (1995) Invasion of *Toxoplasma gondii* occurs by active penetration of the host cell. *J. Cell Sci.*, **108**, 2457–2464.

Pinder,J.C., Fowler,R.E., Dluzewski,A.R., Bannister,L.H., Lavin,F.M., Mitchell,G.H., Wilson,R.J. and Gratzer,W.B. (1998) Actomyosin motor in the merozoite of the malaria parasite, *Plasmodium falciparum*: implications for red cell invasion. *J. Cell Sci.*, **111**, 1831–1839.

Ritchie,M.D., Geeves,M.A., Woodward,S.K. and Manstein,D.J. (1993) Kinetic characterization of a cytoplasmic myosin motor domain expressed in *Dictyostelium discoideum*. *Proc. Natl Acad. Sci. USA*, **90**, 8619–8623.

Ruff,C., Furch,M., Brenner,B., Manstein,D.J. and Meyhöfer,E. (2001) Single-molecule tracking of myosins with genetically engineered amplifier domains. *Nature Struct. Biol.*, **8**, 226–229.

Ruppel,K.M., Uyeda,T.Q. and Spudich,J.A. (1994) Role of highly conserved lysine 130 of myosin motor domain. *In vivo* and *in vitro* characterization of site specifically mutated myosin. *J. Biol. Chem.*, **269**, 18773–18780.

Seeber,F., Beuerle,B. and Schmidt,H.H. (1999) Cloning and functional expression of the calmodulin gene from *Toxoplasma gondii*. *Mol. Biochem. Parasitol.*, **99**, 295–299.

Shaw,M.K. and Tilney,L.G. (1999) Induction of an acrosomal process in *Toxoplasma gondii*: visualization of actin filaments in a protozoan parasite. *Proc. Natl Acad. Sci. USA*, **96**, 9095–9099.

Sibley,L.D., Niesman,I.R., Parmley,S.F. and Cesbron-Delauw,M.F. (1995) Regulated secretion of multi-lamellar vesicles leads to formation of a tubulo-vesicular network in host-cell vacuoles occupied by *Toxoplasma gondii*. *J. Cell Sci.*, **108**, 1669–1677.

Sibley,L.D., Hakansson,S. and Carruthers,V.B. (1998) Gliding motility: an efficient mechanism for cell penetration. *Curr. Biol.*, **8**, R12–R14.

Siemankowski,R.F. and White,H.D. (1984) Kinetics of the interaction between actin, ADP and cardiac myosin-S1. *J. Biol. Chem.*, **259**, 5045–5053.

Spudich,J.A. and Watt,S. (1971) The regulation of rabbit skeletal muscle contraction. I. Biochemical studies of the interaction of the tropomyosin–troponin complex with actin and the proteolytic fragments of myosin. *J. Biol. Chem.*, **246**, 4866–4871.

Sultan,A.A., Thathy,V., Frevert,U., Robson,K.J., Crisanti,A., Nussenzweig, V., Nussenzweig,R.S. and Menard,R. (1997) TRAP is necessary for gliding motility and infectivity of *Plasmodium* sporozoites. *Cell*, **90**, 511–522.

Theriot,J.A. (2000) The polymerization motor. *Traffic*, **1**, 19–28.
Veigel,C., Coluccio,L.M., Jontes,J.D., Sparrow,J.C., Milligan,R.A. and Molloy,J.E. (1999) The motor protein myosin-I produces its working stroke in two steps. *Nature*, **398**, 530–533.
Weeds,A.G. and Taylor,R.S. (1975) Separation of subfragment-1 isoenzymes from rabbit skeletal muscle myosin. *Nature*, **257**, 54–56.
Weiss,S., Chizhov,I. and Geeves,M.A. (2000) A flash photolysis fluorescence/light scattering apparatus for use with sub microgram quantities of muscle proteins. *J. Muscle Res. Cell Motil.*, **21**, 423–432.
Weiss,S., Rossi,R., Pellegrino,M.A., Bottinelli,R. and Geeves,M.A. (2001) Differing ADP release rates from myosin heavy chain isoforms define the shortening velocity of skeletal muscle fibers. *J. Biol. Chem.*, **276**, 45902–45908.
Wells,A.L., Lin,A.W., Chen,L.Q., Safer,D., Cain,S.M., Hasson,T., Carragher,B.O., Milligan,R.A. and Sweeney,H.L. (1999) Myosin VI is an actin-based motor that moves backwards. *Nature*, **401**, 505–508.
West,J.J., Nagy,B. and Gergely,J. (1967) Free adenosine diphosphate as an intermediary in the phosphorylation by creatine phosphate of adenosine diphosphate bound to actin. *J. Biol. Chem.*, **242**, 1140–1145.

Received December 12, 2001; revised February 26, 2002; accepted March 8, 2002